Published in final edited form as:

Magn Reson Imaging. 2015 October ; 33(8): 992–999. doi:10.1016/j.mri.2015.04.008.

Improved Respiratory Navigator Gating for Thoracic 4D flow MRI

Pim van Ooij[1], **Edouard Semaan**[1], **Susanne Schnell**[1], **Shivraman Giri**[2], **Zoran Stankovic**[1], **James Carr**[1], **Alex J. Barker**[1], and **Michael Markl**[1,3]

[1]Department of Radiology, Feinberg School of Medicine, Northwestern University, Chicago, IL, USA

[2]Siemens Healthcare, Chicago, IL, USA

[3]Department of Biomedical Engineering, McCormick School of Engineering, Northwestern University, Chicago, IL, USA

Abstract

Background—Thoracic and abdominal 4D flow MRI is typically acquired in combination with navigator respiration control which can result in highly variable scan efficiency (S_{eff}) and thus total scan time due to inter-individual variability in breathing patterns. The aim of this study was to test the feasibility of an improved respiratory control strategy based on diaphragm navigator gating with fixed S_{eff}, respiratory driven phase encoding, and a navigator training phase.

Methods—4D flow MRI of the thoracic aorta was performed in 10 healthy subjects at 1.5T and 3T systems for the in-vivo assessment of aortic time-resolved 3D blood flow velocities. For each subject, four 4D flow scans (1: conventional navigator gating, 2–4: new implementation with fixed S_{eff} =60%, 80% and 100%) were acquired. Data analysis included semi-quantitative evaluation of image quality of the 4D flow magnitude images (image quality grading on a four point scale), 3D segmentation of the thoracic aorta, and voxel-by-voxel comparisons of systolic 3D flow velocity vector fields between scans.

Results—Conventional navigator gating resulted in variable S_{eff} = 74±13% (range = 56% – 100%) due to inter-individual variability of respiration patterns. For scans 2–4, the the new navigator implementation was able to achieve predictable total scan times with stable $S_{eff,}$ only depending on heart rate. Semi- and fully quantitative analysis of image quality in 4D flow magnitude images was similar for the new navigator scheme compared to conventional navigator gating. For aortic systolic 3D velocities, good agreement was found between all new navigator settings (scan 2–4) with the conventional navigator gating (scan 1) with best performance for S_{eff} = 80% (mean difference = −0.01; limits od agreement = 0.23, Pearson's ρ=0.89, $p < 0.001$). No significant differences for image quality or 3D systolic velocities were found for 1.5T compared to 3T.

Corresponding author: Michael Markl, PhD, Departments of Radiology and Biomedical Engineering, Northwestern University Feinberg School of Medicine, 737 N. Michigan Avenue Suite 1600, Chicago, Illinois 60611, USA, Phone: +1 312-695-1799, mmarkl@northwestren.edu.

Conclusions—The findings of this study demonstrate the feasibility of the new navigator scheme to acquire 4D flow data with more predictable scan time while maintaining image quality and 3D velocity information, which may prove beneficial for clinical applications.

Keywords

Respiration control; navigator gating; 4D flow MRI; aorta

INTRODUCTION

4D flow MRI is a powerful technique to non-invasively measure, visualize and quantify 3D blood flow in the heart and large thoracic and abdominal vessels[1–4]. The technique provides temporal and volumetric (3D) coverage in combination with three-directional velocity encoding[5]. However, the increased coverage results in long total scan times, typically on the order of minutes. For thoracic or abdominal applications, 4D flow MRI is thus typically executed in combination with respiratory gating using bellows[6], self-gating[7], or a navigator signal[6, 8–10] to detect the motion of the lung-liver interface[11].

For conventional navigator-based respiratory gating, an acceptance window ΔW is defined relative to the end-expiratory position, and data is accepted when the breathing position falls within this predefined range. The total scan time is determined by the scan efficiency S_{eff}, i.e. the percentage of data that falls within the navigator acceptance window. Due to inter-individual differences in respiration patterns, however, a fixed navigator acceptance window (ΔW = *constant*) can result in a wide range of S_{eff} thus highly variable total scan time.

The aim of this study was to implement and test a novel navigator gating strategy based on the dynamic adaptation of the lower threshold of the navigator acceptance window in real time to maintain a user selected fixed scan efficiency S_{eff} throughout the entire 4D flow scan. In addition, data was acquired using respiratory ordered phase encoding to allow for increased scan efficiency[1213]. Further, a navigator training phase was included during initial acquisition of outer k-space data, without lengthening the total scan time. We hypothesize that this method can provide more stable scan efficiency S_{eff} for 4D flow MRI for different respiration patterns while maintaining image quality in terms of depiction of vascular geometry in magnitude images as well as 3D blood flow velocity information.

METHODS

Study Cohort

Ten healthy volunteers (age: 47 ± 16 y/o, 23–71 y/o, 8 males, 2 females) with no history of cardiovascular disease, normal aortic valve function and normal thoracic aortic geometry were included in the study. All volunteers provided informed consent. The study was approved by the local Institutional Review Board (IRB) of Northwestern University.

Navigator implementation

Time-resolved 3D phase contrast MRI with three-directional velocity encoding (4D flow MRI) data acquisition was prospectively gated to the ECG cycle as illustrated in figure 1c.

For each time frame within the cardiac cycle, interleaved 3-directional velocity encoding was performed by successively collecting one reference scan and three velocity sensitive scans along x, y, and z direction (i.e. 4TRs were needed to collect the data). K-space segmentation was used to collect a subset (N_{Seg}) of all required ($N_y \times N_z$) phase encoding steps for each time frame. The selection of $N_{Seg} = 2$ resulted in a temporal resolution of $T_{Res} = N_{Seg} * 4TR = 8TR$ and total number of $(N_y \times N_z)/N_{Seg}$ ECG cycles to collect all data.

Navigator gating of the diaphragm motion (figure 1d) was used for image acquisition during free breathing. The navigator pulse (NAV, figure 1c) was played out at the end of each cardiac cycle to update the current respiration phase which was used for respiratory gating. The new navigator strategy is schematically illustrated in figure 1 and combines 1) an initial training phase to determine the optimal navigator acceptance window ΔW for a fixed scan efficiency S_{Eff} (% of data that falls within the gating window) while acquiring outer k-space data, 2) real time-adjustment of the navigator acceptance window to maintain S_{eff} in combination with adaptive phase encoding to minimize respiration artifacts.

1) Training phase—The aim of the training phase was to automatically adjust the navigator acceptance window ΔW based on the fixed scan efficiency S_{eff} while minimizing the impact on initial variability in respiration position on image quality. During the first 10% of the scan, i.e. for the duration of $0.1 \times (N_y \times N_z)/N_{Seg}$ cardiac cycles, only the edges of k_y–k_z-space lines were collected, as illustrated in figure 1a. An initial acceptance window ΔW was specified by the user. The respiration pattern was continuously updated for each cardiac cycle and the lower boundary of ΔW was dynamically adjusted to achieve the fixed scan efficiency S_{eff}. The upper boundary of ΔW was dynamically adjusted each RR-interval by extraction of the maximum position of the lung-liver interface of the past 16 cardiac cycles. As illustrated in figure 1A, the lower acceptance threshold can vary substantially during the initial part of the scan. The influence of this variation on image quality is reduced by filling the edges of k-space during the training phase.

2) Respiratory ordered phase encoding and real time-adjustment of the navigator acceptance window ΔW—As in[13], the remaining k_y–k_z-data were collected according to the position in the respiration cycle to further minimize breathing artifacts. If respiration was within ΔW, the current respiratory position was used to determine the (k_y, k_z)-space position for the following RR-interval. Data acquired near end-expiration (maximum breathing position), where the chest shows the least motion, were assigned to (k_y, k_z) with a small distance from the center of k-space while data measured closer to end-inspiration were assigned to outer k-space. If a k_y–k_z-position was already filled, the phase encode was assigned to an empty phase encode with the closest radius. This process is similar to the previously reported ROPE technique[12] and is schematically illustrated in figure 1b.

As in the training phase, the lower boundary of ΔW was dynamically adjusted to maintain the fixed scan efficiency S_{eff}. At the end of each cardiac cycle the current scan efficiency was determined as

$$S_{\mathrm{Reff}} = \frac{\text{number of accepted } k_y k_z}{\text{number of accepted } k_y k_z + \text{number of rejected } k_y k_z} * 100 \quad (1)$$

When $S_{Reff} > S_{eff}$, ΔW was decreased by increasing the lower acceptance threshold (lower dashed white line in figure 1a and b). As a result, S_{Reff} decreased such that S_{Reff} approached S_{eff}. An increase of the lower edge of ΔW occurred when $S_{Reff} < S_{eff}$ resulting in an increase of S_{Reff}.

MR Imaging

Prospectively ECG gated and navigator controlled 4D flow MRI in a sagittal oblique volume covering the thoracic aorta was performed in n=10 healthy subjects. Data was acquired using 1.5T (n=5 subjects) and 3T (n=5 subjects) systems (MAGNETOM Aera and Skyra, Siemens Medical Solutions, Erlangen, Germany). For each subject, four 4D flow MRI scans were acquired: 1) with conventional navigator gating[13] with fixed ΔW = 16 mm and with the new navigator strategy with 2) S_{eff} set to 60%, 3) S_{eff} = 80% and 4) S_{eff} = 100%.

Pulse sequence parameters for all scans were as follows: spatial resolution = 3.03–3.66mm × 2.13–2.44mm × 2.4–2.7mm; field of view = 340–390mm × 255–315mm, slab thickness = 72–81mm; N_x = 160, N_y = 80, N_z = 30; temporal resolution = 38.4–39.2ms (14–25 time frames); TE/TR/FA = 2.4–2.5ms/4.8–4.9ms/7°; velocity sensitivity (venc) = 150cm/s. All scans were acquired with N_{Seg} = 2 and used parallel imaging (GRAPPA) along the k_y direction with a reduction factor of R = 2 and 24 reference lines (net acceleration factor = 1.7).

Data analysis

Navigator Acceptance & Scan Time—S_{eff} for the conventional navigator implementation was calculated as the average of the navigator acceptance rate over the entire 4D flow scan duration. Total scan times for both the conventional navigator implementation and the new navigator implementation were recorded.

3D Aorta Segmentation—All 4D flow MRI data were corrected for Maxwell terms[14], eddy currents[15] and velocity aliasing using home built software programmed in Matlab (Natick, The Mathworks, USA) as described previously[16]. 3D Phase contrast (PC) magnetic resonance angiography (MRA) data were created by voxel-wise multiplication of the magnitude data with absolute velocities. and subsequent averaging over all cardiac time frames[16]. The 3D PC-MRA images obtained with conventional navigator gating (scan 1) were semi-automatically segmented using a commercial software package (MIMICS, Materialise, Leuven, Belgium). This segmentation served as a 3D mask for all four scans. Peak systole was defined as the cardiac frame with the maximum absolute velocity (averaged over all the voxels in the 3D aorta segmentation).

Semi-Quantitative Evaluation of Image Quality—For each subject, 4D flow magnitude data were independently analyzed by two physicians with two years (E.S) and ten years (Z.S.) of MR imaging experience, blinded to each other's results. Quality assessment was based on a four point scale, with scores between 0 (poor quality) and 3 (best quality) for

edge sharpness, visibility (signal) and noise in the ascending aorta (AAo), aortic arch, supra-aortic arteries (SAA) and the descending aorta (DAo).

Fully Quantitative Evaluation of Image Quality—Edge sharpness was quantified by the calculation of the signal intensity gradient of the peak systolic magnitude images in x-, y- and z-directions. The resulting x-, y- and z-gradient images were subsequently added and masked on the aortic wall based on the 3D aortic segmentation. Visibility (signal) of the aorta in the peak systolic magnitude images was quantified by averaging the signal intensity within the aortic 3D segmentation. Noise in the aorta in the peak systolic magnitude images was quantified by calculating the standard deviation of the signal intensity within the aortic 3D segmentation.

Aortic hemodynamics – 3D Velocity Vector fields—Peak systolic volumetric 3D velocity vector fields for all voxels within the 3D aorta segmentation were generated for all scans and visualized in Matlab (The Mathworks, Natick, MA, USA). To investigate the differences between S_{eff} = 60%, 80% and 100%, the voxel-by-voxel differences of the velocity magnitude between the fixed S_{eff} and the conventional navigator settings were determined.

Statistical analysis

All values are expressed as mean ± SD. To compare the results of semi-quantitative and fully quantitative image grading between all groups (scan 1–4) a Kruskal Wallis test was performed. $P < 0.05$ was considered significant. Voxel-by-voxel differences in velocity magnitude within the 3D aorta segmentation between scans with fixed S_{eff} and conventional navigator gating (scan 1) were evaluated using Bland-Altman analysis. Mean difference and limits of agreement (LOA) were calculated for each comparison[17]. In addition, orthogonal regression[18, 19] was performed to investigate the relationship between fixed S_{eff} and conventional navigator gating. Results are expressed as the Pearson coefficient ρ, a correlation was considered significant for $p < 0.05$.

RESULTS

All four 4D flow acquisitions (conventional navigator, scan 1, and new navigator implementation with fixed S_{eff} = 60%, 80%, and 100%, scans 2–4) were successfully performed and analyzed in all 10 subjects. All scans were acquired with the same number of phase encodes (N_y), number of slices (N_z) and number of segments (N_{seg}) resulting in a total number of 523 heartbeats that were needed to collect all 4D flow data for each scan. The training phase consisted of 52 heartbeats for scans 2–4.

Navigator Acceptance & Scan Time

Table 1 summarizes scan efficiencies and total scan times for all 10 subjects and four scans. As expected, mean S_{eff} for 4D flow MRI with conventional navigator gating (fixed ΔW = 14mm) was highly variable (74 ± 13%, range = 56% – 100%) due to inter-individual variability of respiration patterns. For scans 2–4, the the new navigator implementation was

able to achieve predictable total scan times assuming fixed S_{eff}. Remaining differences between subjects resulted from inter-individual differences in heart rate.

Semi-Quantitative Evaluation of Image Quality

Figure 2 shows representative examples of 4D flow magnitude images for the four different acquisitions (conventional navigator gating, fixed S_{eff} = 60%, 80% and 100%). As summarized in table 2, no significant differences were found for all image quality metrics or between different field strengths.

Fully Quantitative Evaluation of Image Quality

Figure 3 shows representative examples of edge sharpness and visibility/noise images for the four different acquisitions (conventional navigator gating, fixed S_{eff} = 60%, 80% and 100%). As summarized in table 3, no significant differences were found for all image quality metrics.

Aortic hemodynamics – 3D Velocity Vector Fields

Volumetric 3D velocity vector fields inside the 3D segmentation of the aortic lumen were successfully extracted for all subjects and scans of which an example is shown in figure 4. Table 4 summarizes the mean difference and limits of agreements (Bland-Altman analysis) as well as the results of the correlation analysis for all volunteers. Generally good agreement was found between all new navigator settings (scan 2–4) with the conventional navigator gating (scan 1) with best performance for S_{eff} = 80%. Correlation analysis revealed significant relationships in all cases with $P < 0.001$.

DISCUSSION

In this study, 4D flow MRI was combined with a novel respiration control strategy which employed: 1) a training phase in which 10% of k-space data were encoded to outer k-space, 2) respiratory ordered k_y–k_z phase encoding and 3) fixed scan efficiency S_{eff} by continuous adjustment of the navigator acceptance window ΔW. The findings of our volunteer study demonstrate the feasibility of this new respiration control technique to acquire 4D flow MRI data with stable and predictable scan efficiency, while maintaining magnitude image quality and 3D blood flow velocity information.

In comparison to conventional navigator strategies, a fixed scan efficiency was achieved in all cases as selected by the user. Remaining inter-individual differences in scan time were thus only related to differences in heart rate. For a known heart rate, the novel navigator strategy thus allows for predictable total scan times, an important prerequisite to facilitate the integration of 4D flow MRI into a clinical workflow.

The volumetric quantification of aortic hemodynamics showed good agreement between the new and established method for respiration control. The peak systolic 3D velocities for the new navigator strategy with fixes S_{eff} correlated well with the conventional navigator setting for all scans. Then remaining small differences between scans is likely related to the different width of the navigator acceptance window for different S_{eff} and thus different levels

of respiratory blurring. Furthermore, variability in respiration patterns or heart rate between consecutive scans may have led to different velocity values[10]. Another reason for differences between 3D velocity fields between scans 1–4 may be related to the use of the same 3D aorta segmentation for all four scans, disregarding potential subject movement between scans. Another option for analysis would have been to segment the aorta in every scan and subsequently register and interpolate the velocity data to one segmentation (similar to the methodology presented in[20]). However, this approach would have introduced registration and interpolation errors. Physiological changes in flow rate over time could have played a role as well (the sequence of 4D flow scans: conventional, 60%, 80%, 100% was the same for every volunteer).

Nonetheless, differences between the four 4D flow MRI scans for magnitude image quality and velocity vectors were not significant and the differences between S_{eff} = 60%, 80% and 100% were small. Selection of fixed S_{eff} = 80% showed the best agreement with the conventional navigator implementation, but this was not significant compared to S_{eff} = 60% or 100%. The 4D flow MRI measurement with a S_{eff} of 100% may therefore be preferred in clinical 4D flow MRI, to minimize the chances of movement of the patient or the need for general anesthesia. However, the small study cohort underlines the feasibility character of our study. More studies in volunteers with systematically varying breathing patterns as well as in patients with aortic disease are needed to identify the most suitable S_{eff}.

Respiratory gating techniques were originally developed for coronary MRA acquisitions as motion artifacts can degrade image quality of the small coronaries severely. Alongside respiratory gating using bellows[21], respiratory navigator gating[9, 22–25] was developed, which proved more suited for coronary imaging[26]. Coronary MRA keeps driving the development of more advanced respiratory navigator techniques such as retrospective adaptive motion correction[27, 28] and self-navigation[29, 30]. Respiratory navigator gating is generally used for 4D flow MRI as well, as the relatively long scan times make breath-hold acquisitions impractical if not impossible. Other groups have used navigator gating for cardiac tissue phase mapping[31] using a trailing navigator at the end of the cardiac cycle, resulting in 30% to 80% navigator efficiency. Baltes et al.[10] used retrospective motion correction for navigated 2D cine velocity mapping in coronary flow measurements with gating efficiencies ranging from 17–73%. Bieging et al.[32] and Roldán-Alzate et al.[33] used bellows for 4D flow MRI with a 50% efficiency in the aorta and the hepatic vasculature, respectively. Self-navigation was used in the aortic 4D flow MRI study by Uribe et al.[7] leading to a S_{eff} of 40%. Other navigator scan efficiencies found in 4D flow MRI studies range from 42[34] to 64[35]%. We believe that a navigator strategy presented in this study can be beneficial, in terms of stable and higher scan efficiency, for the applications in these studies.

Kozerke et al.[36] were the first to combine 4D flow MRI with respiratory navigator gating. Markl et al. implemented a more efficient navigator gating method combining adaptive k-space reordering and dynamic adjustment of the fixed navigator acceptance window[13]. In both studies, however, the fixed navigator acceptance window led to unstable scan efficiencies. In this study, respiratory navigator gated 4D flow MRI was further improved by showing the feasibility and reproducibility of 4D flow MRI which combines the training phase, adaptive k-space reordering and dynamic real-time adjustment of the acceptance

window, resulting in feasible 4D flow MRI acquisitions with stable scan efficiencies and, for a known heart rate, predictable scan times.

Study Limitations

A disadvantage of the flexible navigator acceptance window is that the navigator acceptance window ΔW window could become wide for high S_{eff}, such that more k-space data during inspiration and less stable chest motion may be encoded compared to the conventional navigator approach. This may lead to increased blurring and breathing artifacts in the images. However, as the results indicate, this was not observed in our study, even at 100% navigator acceptance. Physiological changes in flow rates of the volunteers may have led to the small differences observed in the 4D flow data acquired with the new navigator scheme. For example, the volunteers may have relaxed more over time, or may have fallen asleep, leading to the differences observed in this study. Varying the sequence of the four 4D flow scans could have given more insight on the influence of physiological changes over time. Furthermore, 4D flow MRI test-retest studies are needed to investigate the reliability of the presented method. However, in this study we presented a proof of concept for advanced respiratory navigator gating. Therefore, 4D flow MRI test-retest investigations were outside the scope of this study. Furthermore, a comparison with established breath-held or respiratory gated 2D flow MRI scans could have been performed. However, differences in measured blood flow between 2D and 4D flow MRI acquisitions[37] would likely nullify the effects of the respiratory navigation strategy. Therefore, a comparison with 2D flow MRI acquisitions was outside the scope of the study. A further limitation of this study is the small study cohort and exclusion of patient data. The purpose of this study was to demonstrate the feasibility of the new navigator implementation, which was facilitated by the use of healthy volunteers. The number of subjects was relatively small, which limited the statistical power of the study. However, the study findings were encouraging in the fact that similar trends were found for every volunteer included in the study. Future studies testing the technique in patients with aortic disease are needed to further validate the new navigator scheme.

Another limitation is the investigation of only three navigator settings with a fixed training phase. Training phases of more or less than 10% were not investigated for the sake of simplicity of the study. However, it is not expected that image quality would improve for longer training phases, as the availability of outer k-space will decrease, which will result in k-lines acquired far from the breathing position to be confined to inner k-space. This may lead to decreased image quality. Other limitations include the lack of a comparison with other respiratory navigator techniques such as bellows[32] or self-navigation[7].

In conclusion, a novel implementation of respiratory navigator gating with fixed scan efficiency S_{eff} for 4D flow MRI was successfully applied in a volunteer study. Findings of this study demonstrate the feasibility of the new navigator scheme to acquire 4D flow data with more predictable scan time while maintaining image quality and 3D velocity information. Furthermore, influence of respiratory motion appeared to be limited, indicating the robustness of 4D flow MRI measurements for breathing motion.

Acknowledgments

FUNDING SOURCES: NIH NHLBI grant R01HL115828; NIH grant K25HL119608

References

1. Wigstrom L, Sjoqvist L, Wranne B. Temporally Resolved 3d Phase-Contrast Imaging. Magn Reson Med. 1996; 36:800–803. [PubMed: 8916033]
2. Markl M, Kilner PJ, Ebbers T. Comprehensive 4d Velocity Mapping of the Heart and Great Vessels by Cardiovascular Magnetic Resonance. J Cardiovasc Magn Reson. 2011; 13:7. [PubMed: 21235751]
3. Markl M, Frydrychowicz A, Kozerke S, Hope M, Wieben O. 4d Flow Mri. J Magn Reson Imaging. 2012; 36:1015–1036. [PubMed: 23090914]
4. Stankovic Z, Frydrychowicz A, Csatari Z, Panther E, Deibert P, Euringer W, Kreisel W, Russe M, Bauer S, Langer M, Markl M. Mr-Based Visualization and Quantification of Three-Dimensional Flow Characteristics in the Portal Venous System. J Magn Reson Imaging. 2010; 32:466–475. [PubMed: 20677279]
5. Pelc NJ, Bernstein MA, Shimakawa A, Glover GH. Encoding Strategies for Three-Direction Phase-Contrast Mr Imaging of Flow. Journal of Magnetic Resonance Imaging. 1991; 1:405–413. [PubMed: 1790362]
6. McConnell MV, Khasgiwala VC, Savord BJ, Chen MH, Chuang ML, Edelman RR, Manning WJ. Comparison of Respiratory Suppression Methods and Navigator Locations for Mr Coronary Angiography. American Journal of Roentgenology. 1997; 168:1369–1375. [PubMed: 9129447]
7. Uribe S, Beerbaum P, Sorensen TS, Rasmusson A, Razavi R, Schaeffter T. Four-Dimensional (4d) Flow of the Whole Heart and Great Vessels Using Real-Time Respiratory Self-Gating. Magn Reson Med. 2009; 62:984–992. [PubMed: 19672940]
8. Ehman RL, Felmlee JP. Adaptive Technique for High-Definition Mr Imaging of Moving Structures. Radiology. 1989; 173:255–263. [PubMed: 2781017]
9. Wang Y, Rossman PJ, Grimm RC, Riederer SJ, Ehman RL. Navigator-Echo-Based Real-Time Respiratory Gating and Triggering for Reduction of Respiration Effects in Three-Dimensional Coronary Mr Angiography. Radiology. 1996; 198:55–60. [PubMed: 8539406]
10. Baltes C, Kozerke S, Atkinson D, Boesiger P. Retrospective Respiratory Motion Correction for Navigated Cine Velocity Mapping. J Cardiovasc Magn Reson. 2004; 6:785–792. [PubMed: 15646881]
11. Stuber M, Botnar RM, Danias PG, Kissinger KV, Manning WJ. Submillimeter Three-Dimensional Coronary Mr Angiography with Real-Time Navigator Correction: Comparison of Navigator Locations. Radiology. 1999; 212:579–587. [PubMed: 10429721]
12. Bailes DR, Gilderdale DJ, Bydder GM, Collins AG, Firmin DN. Respiratory Ordered Phase Encoding (Rope): A Method for Reducing Respiratory Motion Artefacts in Mr Imaging. J Comput Assist Tomogr. 1985; 9:835–838. [PubMed: 4019854]
13. Markl M, Harloff A, Bley TA, Zaitsev M, Jung B, Weigang E, Langer M, Hennig J, Frydrychowicz A. Time-Resolved 3d Mr Velocity Mapping at 3t: Improved Navigator-Gated Assessment of Vascular Anatomy and Blood Flow. J Magn Reson Imaging. 2007; 25:824–831. [PubMed: 17345635]
14. Bernstein MA, Zhou XJ, Polzin JA, King KF, Ganin A, Pelc NJ, Glover GH. Concomitant Gradient Terms in Phase Contrast Mr: Analysis and Correction. Magnetic Resonance in Medicine. 1998; 39:300–308. [PubMed: 9469714]
15. Walker PG, Cranney GB, Scheidegger MB, Waseleski G, Pohost GM, Yoganathan AP. Semiautomated Method for Noise Reduction and Background Phase Error Correction in Mr Phase Velocity Data. J Magn Reson Imaging. 1993; 3:521–530. [PubMed: 8324312]
16. Bock J, Kreher W, Hennig J, Markl M. Optimized Pre-Processing of Time-Resolved 2d and 3d Phase Contrast Mri Data. Proc Intl Soc Mag Reson Med. 2007; 15:3138.
17. Bland JM, Altman DG. Statistical Methods for Assessing Agreement between Two Methods of Clinical Measurement. Lancet. 1986; 1:307–310. [PubMed: 2868172]

18. Madansky A. The Fitting of Straight Lines When Both Variables Are Subject to Error. Journal of the American Statistical Association. 1959; 54:173–205.
19. Carroll R, Ruppert D. The Use and Misuse of Orthogonal Regression in Linear Errors-in-Variables Models. The American Statistician. 1996; 50:1–6.
20. van Ooij P, Potters WV, Nederveen AJ, Allen BD, Collins J, Carr J, Malaisrie SC, Markl M, Barker AJ. A Methodology to Detect Abnormal Relative Wall Shear Stress on the Full Surface of the Thoracic Aorta Using 4d Flow Mri. Magnetic Resonance in Medecine. 201410.1002/mrm.25224
21. Ehman RL, McNamara MT, Pallack M, Hricak H, Higgins CB. Magnetic Resonance Imaging with Respiratory Gating: Techniques and Advantages. AJR Am J Roentgenol. 1984; 143:1175–1182. [PubMed: 6333787]
22. Hofman MB, Paschal CB, Li D, Haacke EM, van Rossum AC, Sprenger M. Mri of Coronary Arteries: 2d Breath-Hold Vs 3d Respiratory-Gated Acquisition. J Comput Assist Tomogr. 1995; 19:56–62. [PubMed: 7822549]
23. Post JC, van Rossum AC, Hofman MB, Valk J, Visser CA. Three-Dimensional Respiratory-Gated Mr Angiography of Coronary Arteries: Comparison with Conventional Coronary Angiography. AJR Am J Roentgenol. 1996; 166:1399–1404. [PubMed: 8633453]
24. Muller MF, Fleisch M, Kroeker R, Chatterjee T, Meier B, Vock P. Proximal Coronary Artery Stenosis: Three-Dimensional Mri with Fat Saturation and Navigator Echo. J Magn Reson Imaging. 1997; 7:644–651. [PubMed: 9243382]
25. Oshinski JN, Hofland L, Mukundan S Jr, Dixon WT, Parks WJ, Pettigrew RI. Two-Dimensional Coronary Mr Angiography without Breath Holding. Radiology. 1996; 201:737–743. [PubMed: 8939224]
26. McConnell MV, Khasgiwala VC, Savord BJ, Chen MH, Chuang ML, Edelman RR, Manning WJ. Comparison of Respiratory Suppression Methods and Navigator Locations for Mr Coronary Angiography. AJR Am J Roentgenol. 1997; 168:1369–1375. [PubMed: 9129447]
27. Wang Y, Ehman RL. Retrospective Adaptive Motion Correction for Navigator-Gated 3d Coronary Mr Angiography. J Magn Reson Imaging. 2000; 11:208–214. [PubMed: 10713956]
28. McConnell MV, Khasgiwala VC, Savord BJ, Chen MH, Chuang ML, Edelman RR, Manning WJ. Prospective Adaptive Navigator Correction for Breath-Hold Mr Coronary Angiography. Magn Reson Med. 1997; 37:148–152. [PubMed: 8978644]
29. Stehning C, Bornert P, Nehrke K, Eggers H, Stuber M. Free-Breathing Whole-Heart Coronary Mra with 3d Radial Ssfp and Self-Navigated Image Reconstruction. Magn Reson Med. 2005; 54:476–480. [PubMed: 16032682]
30. Piccini D, Littmann A, Nielles-Vallespin S, Zenge MO. Respiratory Self-Navigation for Whole-Heart Bright-Blood Coronary Mri: Methods for Robust Isolation and Automatic Segmentation of the Blood Pool. Magn Reson Med. 2012; 68:571–579. [PubMed: 22213169]
31. Delfino JG, Johnson KR, Eisner RL, Eder S, Leon AR, Oshinski JN. Three-Directional Myocardial Phase-Contrast Tissue Velocity Mr Imaging with Navigator-Echo Gating: In Vivo and in Vitro Study. Radiology. 2008; 246:917–925. [PubMed: 18223122]
32. Bieging ET, Frydrychowicz A, Wentland A, Landgraf BR, Johnson KM, Wieben O, Francois CJ. In Vivo Three-Dimensional Mr Wall Shear Stress Estimation in Ascending Aortic Dilatation. J Magn Reson Imaging. 2011; 33:589–597. [PubMed: 21563242]
33. Roldan-Alzate A, Frydrychowicz A, Niespodzany E, Landgraf BR, Johnson KM, Wieben O, Reeder SB. In Vivo Validation of 4d Flow Mri for Assessing the Hemodynamics of Portal Hypertension. J Magn Reson Imaging. 2013; 37:1100–1108. [PubMed: 23148034]
34. Clough RE, Waltham M, Giese D, Taylor PR, Schaeffter T. A New Imaging Method for Assessment of Aortic Dissection Using Four-Dimensional Phase Contrast Magnetic Resonance Imaging. J Vasc Surg. 2012; 55:914–923. [PubMed: 22386146]
35. Sigfridsson A, Petersson S, Carlhäll C-J, Ebbers T. Four-Dimensional Flow Mri Using Spiral Acquisition. Magnetic Resonance in Medicine. 2012; 68:1065–1073. [PubMed: 22161650]
36. Kozerke S, Hasenkam JM, Pedersen EM, Boesiger P. Visualization of Flow Patterns Distal to Aortic Valve Prostheses in Humans Using a Fast Approach for Cine 3d Velocity Mapping. J Magn Reson Imaging. 2001; 13:690–698. [PubMed: 11329190]

37. Stalder A, Russe M, Frydrychowicz A, Bock J, Hennig J, Markl M. Quantitative 2d and 3d Phase Contrast Mri: Optimized Analysis of Blood Flow and Vessel Wall Parameters. Magn Reson Med. 2008; 60:1218–1231. [PubMed: 18956416]

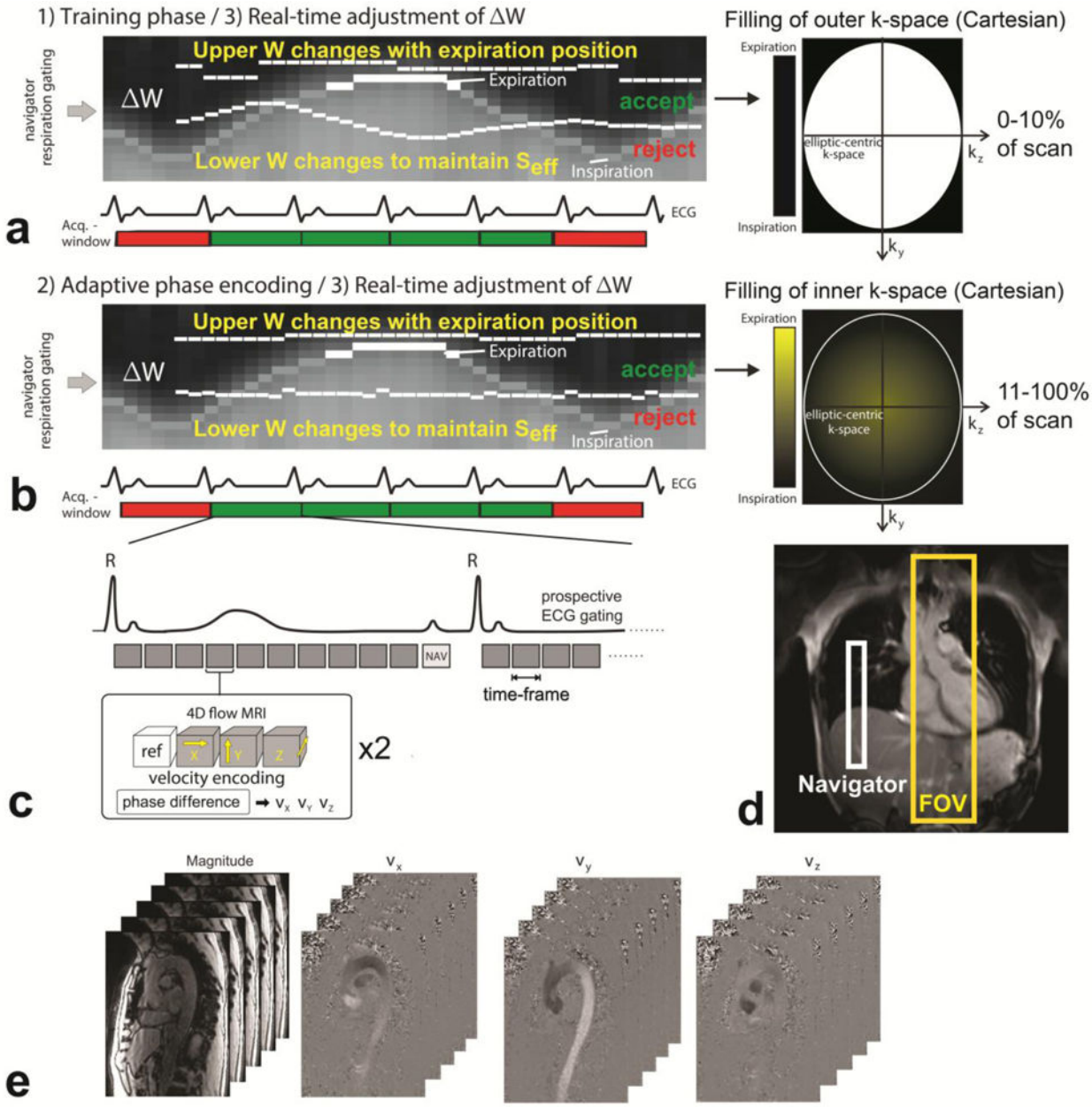

Figure 1.

Data acquisition with prospective ECG gating and respiratory navigator gating consisting of (a) a training phase for the initial adjustment of the navigator acceptance window (ΔW) during the collection of the initial 10% of the total 4D flow data during acquisition of outer k_y–k_z-space and (b) continued real time adjustment of ΔW in combination with respiratory driven phase encoding for the remaining 90% of data acquisition. (c) The 4D flow scan was prospectively ECG gated and for each time-frame, four datasets, one reference scan and three flow-sensitive scans, were acquired in an interleaved fashion. (d) The navigator was placed on the lung-liver interface, and the field of view (FOV) covered the entire thoracic aorta. (e) The resulting 4D flow data consisted of time resolved 3D magnitude data, and

three time-resolved 3D phase difference datasets representing blood flow velocity in x, y and z-direction.

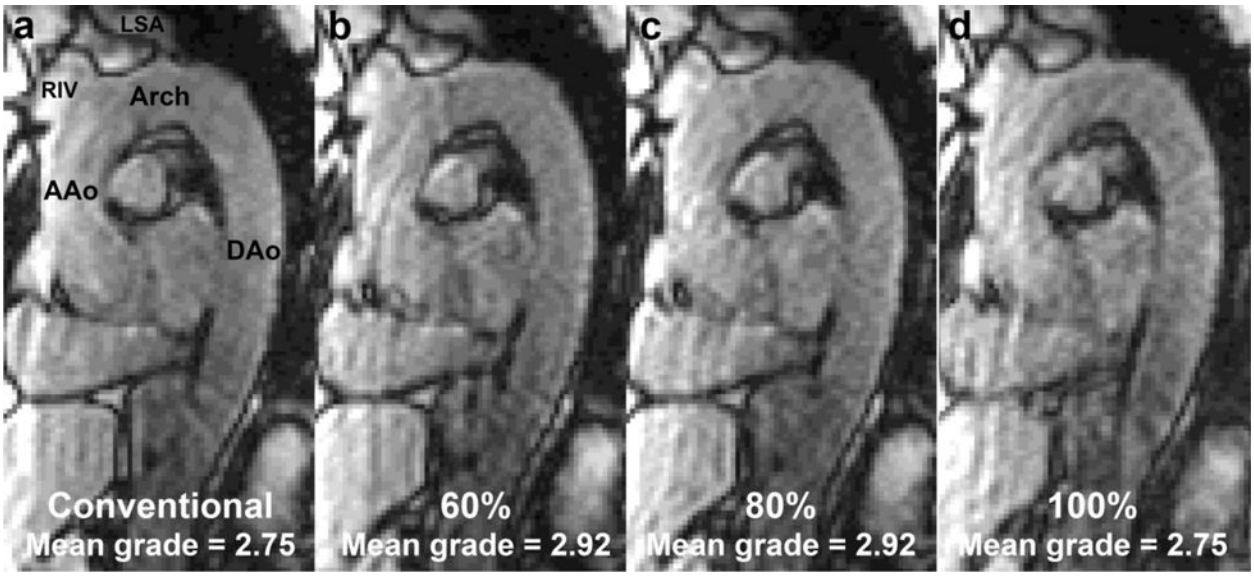

Figure 2.

Typical (volunteer 2, 1.5T) 4D flow magnitude images with (a) conventional navigator gating, fixed S_{eff} = (b) 60%, (c) 80% and (d) 100%. Image quality grading was averaged over categories and observers. Indicated are the ascending aorta (AAo), the aortic arch (Arch), the descending aorta (DAo), the right innominate vein (RIV) and the left subclavian artery (LSA).

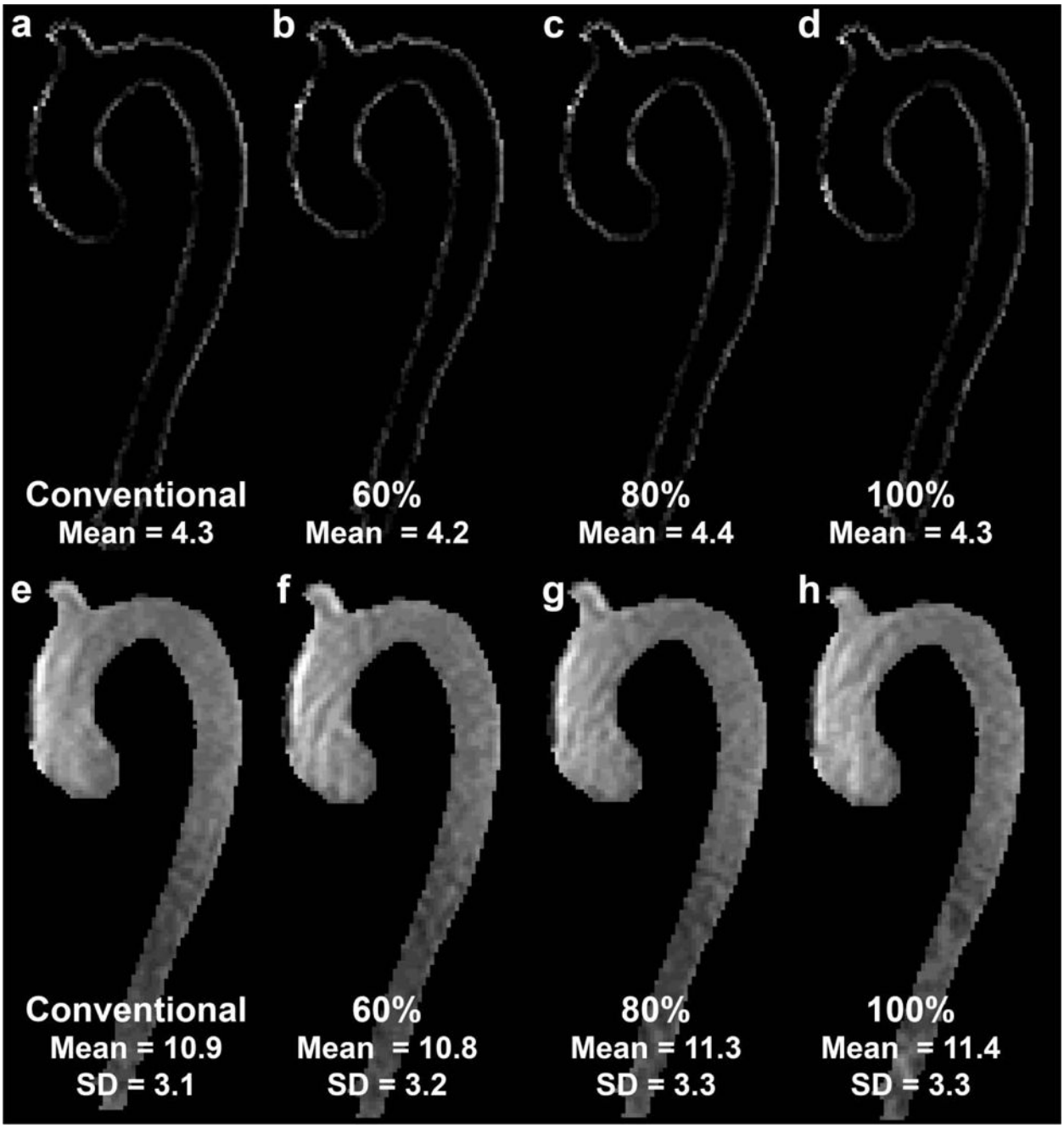

Figure 3.

Typical (volunteer 2, 1.5T) images for magnitude edge sharpness (top row) with (a) conventional navigator gating, fixed S_{eff} = (b) 60%, (c) 80% and (d) 100%. Bottom row: visibility (signal, mean) and noise (standard deviation SD) images for the same volunteer with (a) conventional navigator gating, fixed S_{eff} = (b) 60%, (c) 80% and (d) 100%.

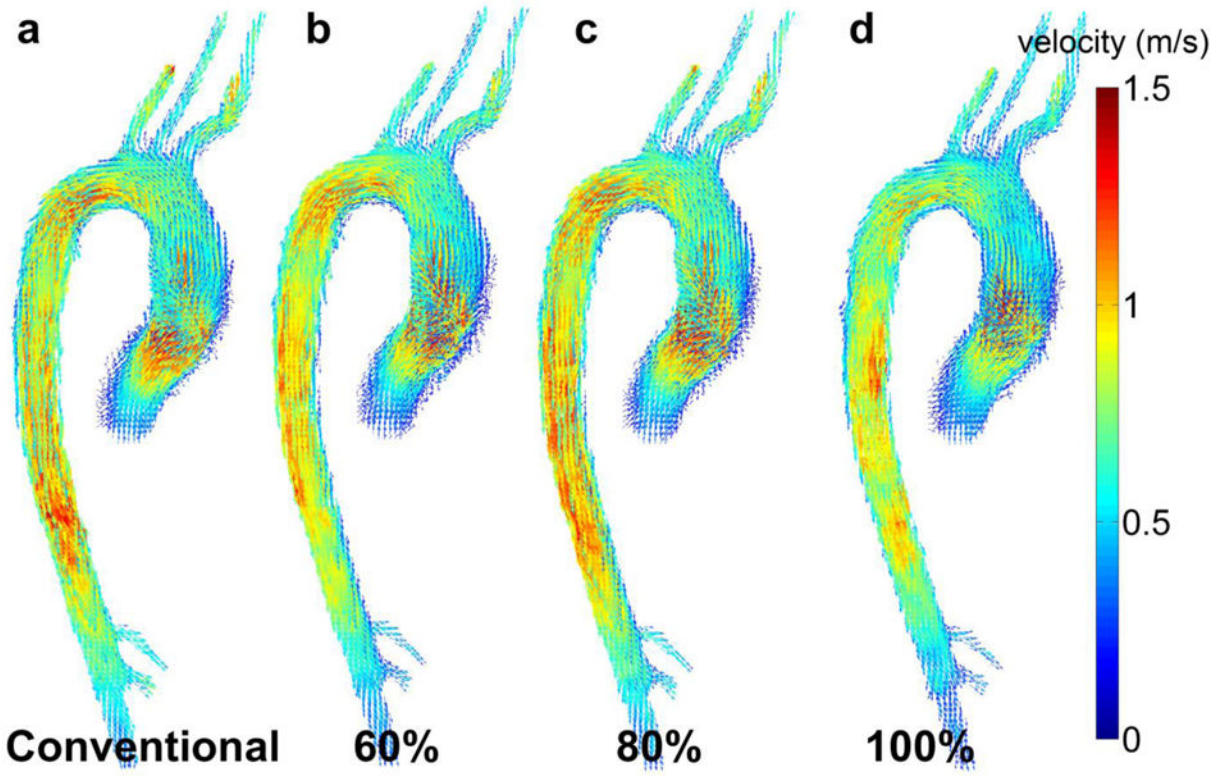

Figure 4.

Examples (volunteer 7, 3T) for 3D velocity vector images at peak systole for (a) conventional navigator (scan 1) gating and for the new navigator scheme (scans 2–4) with fixed S_{eff} = (b) 60%, (c) 80% and (d) 100%.

Table 1

Scan efficiency for conventional navigator gating and total scan times for scans 1–4

Subject	Scan efficiency S_{eff} [%]	Total 4D flow scan time [s]			
	Conventional	1) Conventional	2) S_{eff}=60%	3) S_{eff}=80%	4) S_{eff}=100%
1	69	468	538	407	347
2	56	856	782	590	483
3	78	740	987	759	617
4	71	708	830	641	513
5	73	653	833	613	458
6	100	531	913	669	539
7	68	574	716	531	384
8	91	686	1014	738	613
9	72	642	728	578	457
10	59	665	659	483	413

Magn Reson Imaging. Author manuscript; available in PMC 2016 October 01.

Table 2

Semi-quantitate analysis of 4D flow magnitude data image quality for 1.5T (5 subjects) and 3T (5 subjects) and all subjects combined (Total).

		Conventional navigator			S_{eff}=60%			S_{eff}=80%			S_{eff}=100%			*P*-value
		1.5T	3T	Total	1.5T	3T	Total	1.5T	3T	Total	1.5T	3T	Total	Total*
Edge sharpness	**AAo**	2.4±0.2	2.2±0.3	2.3±0.3	2.4±0.2	2.2±0.3	2.3±0.3	2.4±0.2	2.2±0.3	2.3±0.3	2.4±0.2	2.1±0.2	2.3±0.3	0.96
	arch	2.6±0.2	2.2±0.3	2.4±0.3	2.6±0.2	2.2±0.3	2.4±0.3	2.6±0.2	2.2±0.3	2.4±0.3	2.6±0.2	2.1±0.2	2.3±0.3	0.97
	SAA	2.2±0.7	1.9±0.6	2.1±0.6	2.3±0.6	1.9±0.6	2.1±0.6	2.3±0.6	1.9±0.6	2.1±0.6	2.2±0.7	1.6±0.4	1.9±0.6	0.80
	DAo	2.6±0.2	2.2±0.3	2.4±0.3	2.6±0.2	2.2±0.3	2.4±0.3	2.6±0.2	2.3±0.3	2.5±0.3	2.6±0.2	2.1±0.2	2.4±0.3	0.89
Visibility	**AAo**	3.0±0.0	2.7±0.3	2.9±0.2	3.0±0.0	2.7±0.3	2.9±0.2	3.0±0.0	2.7±0.3	2.9±0.2	3.0±0.0	2.7±0.3	2.9±0.2	1.00
	arch	3.0±0.0	2.7±0.3	2.9±0.2	3.0±0.0	2.7±0.3	2.9±0.2	3.0±0.0	2.7±0.3	2.9±0.2	3.0±0.0	2.7±0.3	2.9±0.2	1.00
	SAA	2.3±0.3	1.8±0.3	2.1±0.4	2.4±0.2	1.8±0.3	2.1±0.4	2.4±0.2	1.7±0.3	2.1±0.4	2.3±0.3	1.7±0.3	2.0±0.4	0.95
	DAo	3.0±0.0	2.7±0.3	2.9±0.2	3.0±0.0	2.7±0.3	2.9±0.2	3.0±0.0	2.7±0.3	2.9±0.2	3.0±0.0	2.7±0.3	2.9±0.2	1.00
Noise	**AAo**	2.5±0.4	2.4±0.2	2.5±0.3	2.7±0.5	2.4±0.2	2.6±0.4	2.6±0.4	2.4±0.2	2.5±0.3	2.5±0.4	2.5±0.4	2.5±0.3	0.92
	arch	2.5±0.0	2.3±0.3	2.4±0.2	2.7±0.3	2.4±0.2	2.6±0.3	2.6±0.2	2.4±0.2	2.5±0.2	2.5±0.0	2.5±0.4	2.5±0.2	0.56
	SAA	2.4±0.2	2.5±0.4	2.5±0.3	2.6±0.4	2.5±0.4	2.6±0.4	2.5±0.4	2.5±0.4	2.5±0.3	2.4±0.2	2.6±0.4	2.5±0.3	0.92
	DAo	2.5±0.0	2.3±0.3	2.4±0.2	2.8±0.3	2.4±0.2	2.6±0.3	2.6±0.2	2.4±0.2	2.5±0.2	2.5±0.0	2.5±0.4	2.5±0.2	0.56
mean ± SD		2.6±0.3	2.3±0.3	2.5±0.3	2.7±0.2	2.3±0.3	2.5±0.3	2.6±0.2	2.3±0.3	2.5±0.3	2.6±0.3	2.3±0.4	2.5±0.3	0.36

The individual numbers represent mean ± SD of scores averaged over both observers and subjects. SD = Standard deviation, SAA = supra-aortic arteries, AAo = ascending aorta DAo = descending aorta

*indicates multiple comparisons between all four scans, Kruskal-Wallis test.

Table 3

Fully quantitative analysis of 4D flow magnitude data image quality for 1.5T (5 subjects) and 3T (5 subjects) and all subjects combined (Total).

	Conventional navigator			S_{eff}=60%			S_{eff}=80%			S_{eff}=100%			*P*-value
	1.5T	**3T**	**Total**	**1.5T**	**3T**	**Total**	**1.5T**	**3T**	**Total**	**1.5T**	**3T**	**Total**	**Total***
Edge sharpness	4.1±0.4	6.6±1.7	5.3±1.8	4.0±0.4	6.6±1.9	5.3±1.9	4.0±0.4	6.6±1.8	5.3±1.9	3.9±0.6	6.4±1.5	5.2±1.7	0.99
Visibility (mean signal)	11±1	24±5	18±8	11±1	25±6	18±9	11±1	25±5	18±8	11.1±	25±5	18±8	1.00
Noise (SD signal)	2.9±0.4	6.6±2.0	4.8±2.4	3.0±0.6	6.6±2.0	4.8±2.3	3.0±0.4	6.8±2.1	4.9±2.5	3.1±0.7	6.6±1.8	4.8±2.2	1.00

The individual numbers represent mean ± SD averaged over all subjects. SD = Standard deviation.

*indicates multiple comparisons between all four scans, Kruskal-Wallis test.

Table 4

Results of Bland Altman analysis (mean difference, limits of agreement, LOA) and orthogonal regression analysis (Pearson's ρ, slope, intercept) aortic peak systolic velocities analysis for 1.5T (5 subjects) and 3T (5 subjects) and all subjects combined (Total).

	Mean difference [m/s]			LOA [m/s]			Pearson's ρ		
S_{eff}	1.5T	3T	Total	1.5T	3T	Total	1.5T	3T	Total
60%	−0.03±0.06	0.03±0.03	−0.00±0.06	0.28±0.03	0.25±0.07	0.27±0.05	0.79±0.08	0.89±0.05	0.84±0.08
80%	−0.04±0.06	0.01±0.02	−0.01±0.06	0.25±0.03	0.21±0.06	0.23±0.04	0.84±0.03	0.92±0.03	0.89±0.05
100%	−0.02±0.07	0.09±0.04	0.02±0.07	0.30±0.03	0.25±0.05	0.28±0.05	0.77±0.04	0.89±0.03	0.83±0.07

For each fixed S_{eff} (60%, 80%, 100%) the voxel-by-voxel velocity magnitude difference between scans with the fixed S_{eff} and the conventional navigator setting was analyzed. Correlation analysis revealed significant relationships in all cases with $P < 0.001$.